Optical Properties of GeSe$_{1-x}$Te$_x$ Chalcogenide Materials Promising for on-Chip Low and Ultra-Low Loss Reconfigurable Photonics and Nonlinear Devices

Anthony Albanese, Martina Tomelleri, Lara Karam, Jean-Baptiste Dory, Christophe Licitra, Benoît Charbonnier, Jean-Baptiste Jager, Aurélien Coillet, Benoît Cluzel, and Pierre Noé*

The highly promising linear and nonlinear optical properties of innovative thin films of GeSe$_{1-x}$Te$_x$ chalcogenide materials in the amorphous as-deposited state, and after crystallization, are revealed here. These innovative alloys bridge the gap between two families of materials: chalcogenide glasses (GeSe) and phase-change materials (GeTe). Their unique optical properties make them attractive candidates for reconfigurable and nonlinear photonic applications in the infrared. In this context, it is shown how, by varying the Te content of GeSe$_{1-x}$Te$_x$ thin films, it is possible to tailor their linear and nonlinear optical properties to optimize them for a wide range of innovative applications.

1. Introduction

Chalcogenide materials have been widely studied for a long time owing to their uncommon electronic, structural, and optical properties. This unique portfolio of properties has led to their use for a wide number of applications, ranging from infrared (IR) optics to nonlinear photonics as well as nonvolatile memory devices.[1–6] Among the large family of chalcogenides, the

A. Albanese, M. Tomelleri, L. Karam, J.-B. Dory, C. Licitra, B. Charbonnier, P. Noé
Université Grenoble Alpes
CEA, LETI
F-38000 Grenoble, France
E-mail: pierre.noe@cea.fr

J.-B. Jager
Université Grenoble Alpes
CEA, IRIG
F-38000 Grenoble, France

A. Coillet, B. Cluzel
ICB, UMR CNRS 6303
Université de Bourgogne
F-21078 Dijon, France

The ORCID identification number(s) for the author(s) of this article can be found under https://doi.org/10.1002/pssr.202400129.

growing demand for increasingly functional photonic devices has seen phase-change materials (PCMs) cement themselves as attractive electro-optically active materials,[7,8] nanophotonic components,[9,10] and metasurfaces.[11–16] Thanks to a large and unique contrast of optical properties, arising from a reversible and nonvolatile amorphous-to-crystalline phase transition, PCMs can be integrated as the tunable medium in different optical devices such as optical filters, phase shifters, switches, modulators, couplers, multiplexers, or multipliers[17–19] to name just a few.

The most studied material among the PCMs is the Ge$_2$Sb$_2$Te$_5$ (GST225), lying on the GeTe-Sb$_2$Te$_3$ pseudo-binary line of the Ge–Sb–Te ternary phase diagram. This alloy has been widely studied for years in the frame of optical data storage such as CD-RW, DVD-RAM, and Blu-ray disks.[1,20,21] The interest of this alloy is the result, first, of its relatively low crystallization temperature ($T_x \approx 150$–$180\,°C$), second, of its huge refractive index contrast in the visible range achieved upon switching from amorphous to face-centered cubic (fcc) crystalline phase driven by laser pulses applications ($n_{fcc}^{GST225} - n_{am}^{GST225} = 2.97$ at 1550 nm). However, at telecommunication wavelengths (1.55 μm), GST225 exhibits values of the extinction coefficient k which are increasing by one order of magnitude (from ≈ 0.1 to ≈ 1.5) upon crystallization which is particularly detrimental for most of the applications in integrated photonics. Therefore, in this spectral range, new PCMs with large Δn and small Δk are desired to maximize their impact as a tunable optical media reported on a photonic platform but with minimal loss level. In this field, to compare candidate PCMs, a material figure of merit (FOM) that quantitatively correlates with the insertion loss and contrast ratio in optical devices[22] is used and defined as:

$$\text{FOM} = \frac{\Delta n}{\Delta k} \tag{1}$$

where $\Delta n = n_{cr} - n_{am}$ and $\Delta k = k_{cr} - k_{am}$, with n and k refractive index and extinction coefficient of the amorphous (am) and crystalline (cr) phase, respectively. For standard GST225 thin films, FOM is 2.2 at 1.55 μm for the fcc phase while higher FOM values were reported for other alloys such as GeTe (FOM ≈ 6.2) and Ge$_2$Sb$_2$Se$_4$Te$_1$ (FOM ≈ 4.2).[17,23–25]

Chalcogenide glasses have also attracted significant interest for decades[26,27] thanks to a high transparency window in the infrared range combined with large third-order susceptibility $\chi^{(3)}$,[28–32] which make them serious candidates for developing on-chip nonlinear photonics applications. In this case, a trade-off on the material structure has to be found between the stability of the amorphous phase, which minimizes the material photosensitivity but also tends to reduce nonlinear polarizability, and the introduction of alloying elements, which favor the latter to the detriment of the phase stability.[33,34] Despite this narrow guideline, chalcogenide glasses have been successfully implemented in innovative mid-infrared (MIR) components such as MIR supercontinuum (SC) laser sources, optical sensors for gas spectroscopy, real-time monitoring of glucose levels, IR microlens arrays and all-optical integrated circuits.[5,32,35–37] For nonlinear applications based on the large third-order susceptibility $\chi^{(3)}$ of chalcogenide glasses, the Kerr refractive index (n_2) characterizes the optical nonlinearity of the material. It has been deeply investigated by Sheik-Bahae et al. who proposed a model for its theoretical calculation.[38] In previous publications, we have shown that this model is robust in predicting n_2 over a wide variety of $GeSb_wS_xSe_yTe_z$ amorphous chalcogenide compositions for 1.55 μm wavelength applications, finding excellent agreement with experiments.[33,34,39]

In conjunction with these previous works in optics and photonics, Tomelleri et al. showed that the electronic and structural properties of $GeSe_{1−x}Te_x$ thin films are unique thanks to an unprecedented change of electronic properties when switching from the amorphous to the crystalline state and exhibit exceptional thermal stability of the amorphous phase.[40] These alloys combine the properties of GeSe which has a covalently bonded orthorhombic crystalline phase responsible for a very small (but still present) contrast of electronic properties upon crystallization of the amorphous phase at high temperature (≈385 °C) to that of GeTe which is a prototypical PCM with a rhombohedral structure proposed to be "metavalently bonded". Indeed, the latter shows an uncommon contrast of properties with its covalently bonded amorphous counterpart.[40–46] Such a "metavalent" bonding (MVB) mechanism can be described as lying in between covalent and metallic bonding explaining the high electronic conductivity of the crystalline phase of the PCMs (several orders of magnitude higher than that of the insulating amorphous phase) and its high electronic polarizability. The latter results in high optical dielectric constants and it is also at the origin of the large optical properties contrast between the amorphous and crystalline states of PCMs. These MVB materials are characterized by a high chemical bond polarizability evidenced by a high Born effective charge, as well as uncommon vibrational properties such as phonon softening and large Grüneisen parameters.[41–45] In addition, Se-rich $GeSe_{1−x}Te_x$ thin films have amorphous phase thermal stability against unwanted crystallization of up to 10 years at 272 °C for $x ≈ 0.16$.[40] This exceptional combination of properties for a homogeneous alloy also occurs without any phase segregation upon crystallization, which makes these films extremely promising for integration into embedded memory devices and for instance in the automotive industry. Besides, their high amorphous phase stability, demonstrated by the high crystallization temperature of some $GeSe_{1−x}Te_x$ compositions ($T_x > 250$ °C for $0 < x < 0.72$), is of particular interest for their use in the glassy state for nonlinear on-chip photonic devices working in the IR range.[33,34,47,48] However, their linear and nonlinear optical properties have not been reported yet.

In this context, the linear and nonlinear optical properties of innovative $GeSe_{1−x}Te_x$ thin films are reported here and discussed accordingly to envision on-chip applications in programmable and/or nonlinear photonics. All the films were deposited by means of magnetron cosputtering, starting from pure GeSe and GeTe targets to obtain films with compositions lying on the GeSe-GeTe pseudo-binary line of the Ge–Se–Te ternary phase diagram. Finally, we provide general guidelines for elaborating $GeSe_{1−x}Te_x$ thin films with outstanding properties regarding the envisioned application.

2. Results and Discussion

To assess the impact of the Te content on the optical properties of the $GeSe_{1−x}Te_x$ thin films, we first determined their linear optical constants by means of variable angle spectroscopic ellipsometry (VASE) in the range (210–2500 nm). **Figure 1** shows the linear optical refractive index n and the extinction coefficient k, as a function of wavelength for the amorphous as-deposited $GeSe_{1−x}Te_x$ samples. On the same graphs, the optical properties of GST225 are plotted in dashed lines and serve as a reference. GST225 and GeTe films, elaborated under the same conditions as $GeSe_{1−x}Te_x$, exhibit optical properties in good agreement with the literature[23,41,49–55] which assesses that the results reported here can be widely generalized. Above the interband absorption wavelength, at long wavelength, n tends to plateau while k decreases drastically. Furthermore, n increases with the Te atomic percent (at%) which is due to the decrease of the energy gap E_g and by the fact that the substitution of Se by Te atoms makes the material more polarizable. A similar behavior was reported in literature for thin films of $Ge_{10}Se_{90−x}Te_x$, $Ge_{12.5}Se_{87.5−x}Te_x$, and $Ge_{30}Se_{70−x}Te_x$ when the Te content increases.[56–58] Regarding the extinction coefficient k, above the interband absorption region, it progressively increases with Te at% from GeSe to GeTe. The reference GST225 presents the highest k values up to 1700 nm. At 1550 nm, it is also worth noting that GeSe shows a very low k value $<10^{−4}$ (limit attained by VASE measurements modeling, see Experimental Section), while $k = 0.13$ and 0.15 are measured for GeTe and GST225, respectively.

In **Figure 2**, we plot n and k as a function of wavelength for the thin films after crystallization by annealing the samples up to 400 °C (250 °C for crystalline fcc GST225) using a heating ramp rate of 10 °C min$^{−1}$. Apart from GeSe that will be discussed later, all the compounds exhibit a pronounced increase in the refractive index after crystallization ($\Delta n > 1.7$). As for amorphous phases, n increases with the Te concentration. The crystalline $GeSe_{0.7}Te_{0.3}$ thin film shows the lowest $n = 5.10$ at 1550 nm, while GeTe and GST225 have refractive indices $n = 6.75$ and $n = 7.55$ at the same wavelength, respectively. Note that for all $GeSe_{1−x}Te_x$ films with $x \neq 0$, a Drude contribution appears with an increase of k values at wavelengths longer than ≈1.7 μm. The GST225 reference thin film does not show any visible Drude contribution in the studied range in agreement with previous literature showing its appearance for wavelengths above 2500 nm[24,59–61] (see Experimental Section for more details).
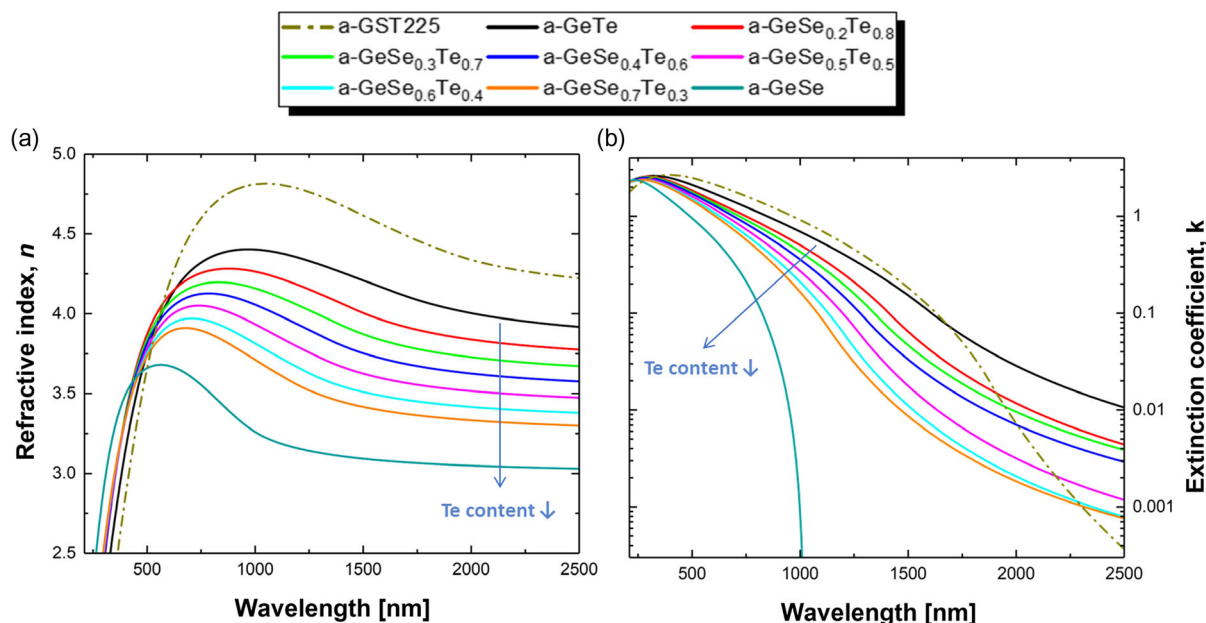
Figure 1. a) Linear refractive index (*n*) and b) extinction coefficient (*k*) as a function of wavelength for the amorphous as-deposited $GeSe_{1-x}Te_x$ (continuous) and GST225 (dashed) thin films (≈50 nm thick) obtained by means of VASE data modeling (for details see text and Experimental Section). *k* is plotted using a logarithmic scale for the purpose of clarity.
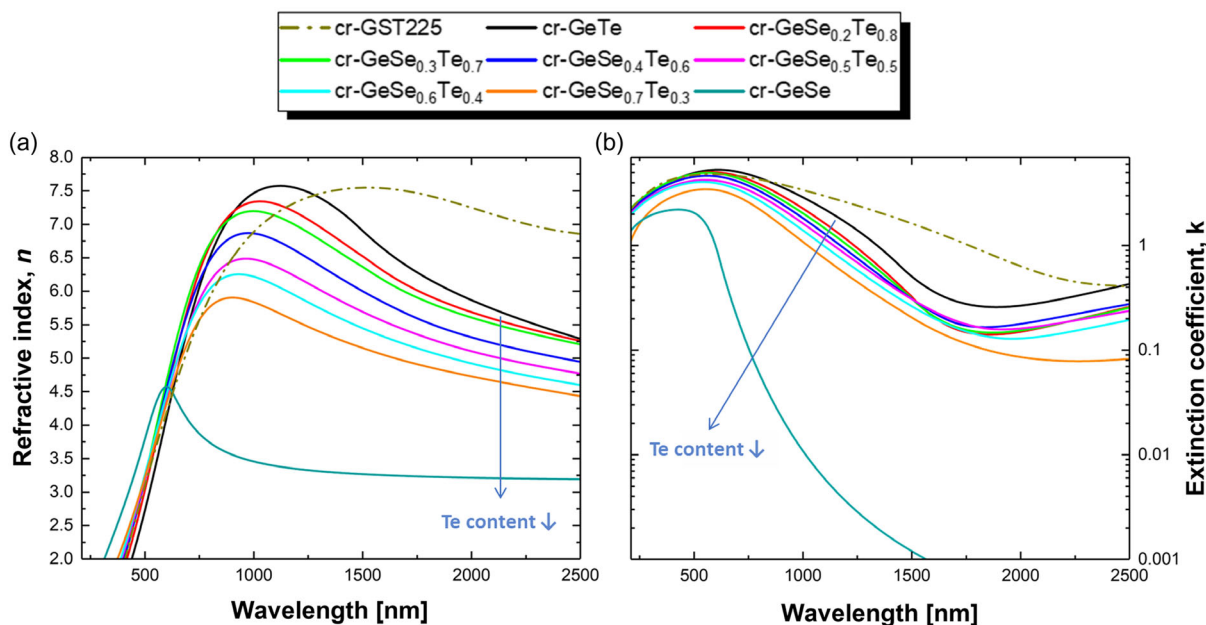
Figure 2. a) Linear refractive index (*n*) and b) extinction coefficient (*k*) as a function of wavelength for the crystalline $GeSe_{1-x}Te_x$ (continuous) and GST225 (dashed) thin films (≈50 nm thick) obtained by VASE data modeling (for details see text and Experimental Section). *k* is plotted using a logarithmic scale for the purpose of clarity. The modeled *n* and *k* of the crystalline GeSe thin film are "effective optical constants" that also consider the air due to the voids that the thin film shows after crystallization due to volume change upon phase transition (see text and Supporting Information).

For a deeper analysis, the real part of the dielectric function ε_1 for both the amorphous and the crystalline phases can be retrieved from SE raw data (see the Supporting Information) and extrapolated at 2500 nm for the different $GeSe_{1-x}Te_x$ samples (with Drude contribution subtraction when present). Retrieved values of ε_r quantitatively agree with the ε_∞ of Guarneri et al.[43] who measured them modeling the results they obtained by means of reflectance spectra (see the Supporting Information).

Our results in Figure 1 and 2 demonstrate that all $GeSe_{1-x}Te_x$ compositions exhibit lower losses than GST225 while keeping a good contrast of refractive index between the amorphous and the crystalline phase at 1550 nm, a wavelength critical for numerous programmable photonic applications. Thus, we calculated the FOM of all the thin films from VASE data, and we plotted its spectral evolution in **Figure 3**. Apart from GeSe, for which the FOM diverges to infinite because of almost zero absorption in both phases, the FOM of all $GeSe_{1-x}Te_x$ with $x \neq 0$ compositions is higher than that of GST225. At 1550 nm, the best FOM is found to be 12.1 for $GeSe_{0.2}Te_{0.8}$ which is 550% higher than GST225. Moreover, all the studied compositions show very large FOM values compared to the other materials in the literature. Besides, $GeSe_{0.3}Te_{0.7}$ has a FOM equal to 11.3, while GeTe is found to have a FOM = 8.7 at 1.55 µm. For comparison, $Ge_2Sb_2Se_4Te_1$ (GSST2241) reported in ref. [23] and presented as a high-performance material compared to GST225 has a FOM value of 4.2, resulting from $\Delta n = 1.8$ and $\Delta k = 0.4$ at 1550 nm. By comparison, $GeSe_{0.2}Te_{0.8}$ has a FOM almost 3 times higher, with $\Delta n = 2.4$ and $\Delta k = 0.2$. All $GeSe_{1-x}Te_x$ with $x \neq 0$ compositions follow this trend and controlling the Se/Te content allows tailoring the alloys' properties depending on the desired applications. It is also remarkable that all the alloys reported here are very promising for 2 µm applications which is a fast-growing wavelength for optical communications.[62] Indeed, Soref et al.[62] have proposed that a new generation of low-loss fibers carrying optical signals at wavelengths of 1.9–2.1 µm could serve as a useful complement or adjunct to the current telecoms infrastructure working at 1.55 µm, which is becoming increasingly congested. At this wavelength, the FOM of GST225 was showed to be 4.7, while for $GeSe_{1-x}Te_x$ with $x \neq 0$ thin films, the FOM values at 2 µm range from 16.6 for $GeSe_{0.7}Te_{0.3}$, to 7.8 for GeTe. For longer wavelengths in the mid-infrared (MIR), the FOM values exhibit a decline mainly caused by the increase of the Drude absorption in the crystalline phase of the thin films.

Additionally, for applications requiring zero absorption, such as phase shifters or modulators, GeSe may appear as a good candidate. In fact, its extinction coefficient tends to 0 in both amorphous and crystalline phases, as shown in Figure 1b and 2b. Therefore, GeSe can be considered as ultra-low loss material with very promising phase-change properties for pure optical phase modulation on a chip. However, this must be mitigated by the fact that, in this case, the modeled refractive index and extinction coefficient of the crystalline GeSe thin film are "effective optical constants" that also take into account the air due to voids that the thin film presents after crystallization due to the volume change during the phase transition (see Supporting Information). As a result, the refractive index and the extinction coefficient of the crystalline phase could be higher than those we have measured over a large area of thin film using VASE, and further optical evaluations and characterizations are in progress. Deposition in the crystalline state of the films would be a good solution to prevent the formation of voids during the crystallization of the amorphous thin films. This could not be carried out in the 300 mm industrial deposition tool used in this study, as the deposition chamber was not equipped with a heating sample holder but it will be the subject of future work. Note that PCMs such as Sb_2S_3 and Sb_2Se_3 were presented in recent publications[61,63,64] and showed ultra-low loss characteristics. At 1550 nm, Sb_2S_3 exhibits a refractive index difference between its amorphous and crystalline phases ranging from $\Delta n = 0.3$ to $\Delta n = 0.9$[61,63,64] depending on deposition stoichiometry and sample thickness. Sb_2Se_3 showed $\Delta n = 0.77$[63]
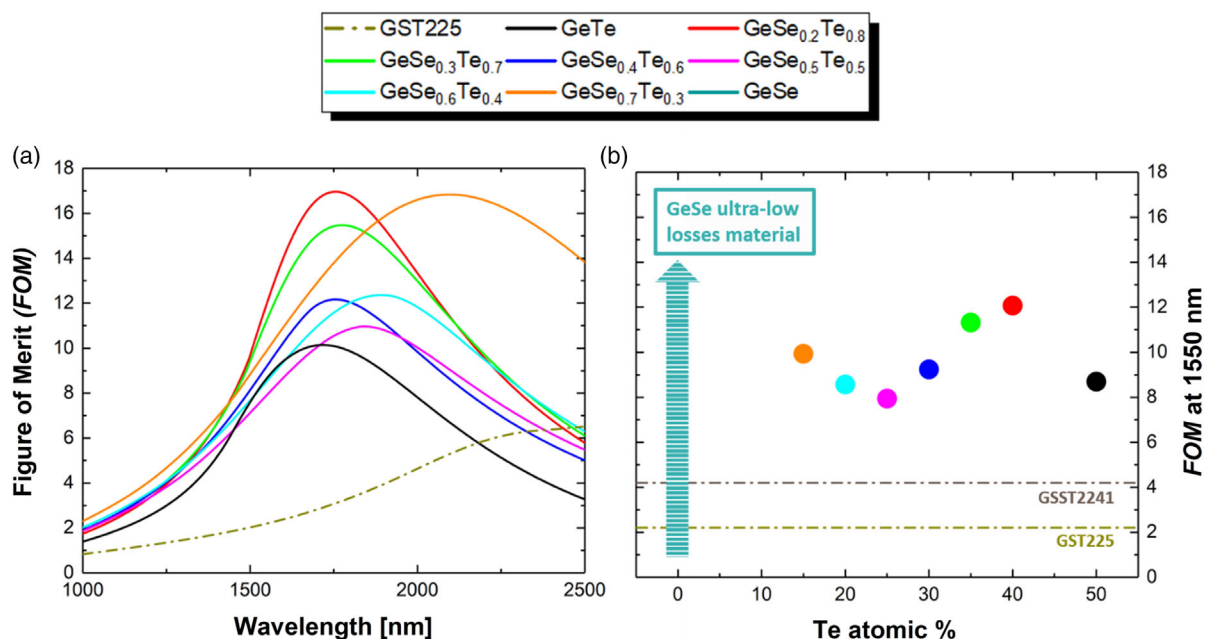
Figure 3. a) FOM $= \frac{\Delta n}{\Delta k}$ as a function of wavelength and b) focus at 1550 nm for the $GeSe_{1-x}Te_x$ and GST225 thin films. All the $GeSe_{1-x}Te_x$ thin films have a FOM higher than the GST225 and GSST2241 reference materials. To be noticed, GeSe film is not plotted in a) because the as-defined FOM value tends to be infinite. In fact, for this material, Δk tends to zero (see text for details).

ADVANCED SCIENCE NEWS
www.advancedsciencenews.com

pss rrl
physica status solidi
www.pss-rapid.com

or $\Delta n = 0.74$.[61] These values are higher than the $\Delta n = 0.2$ of the GeSe thin film we showed, but GeSe could offer an alternative and further exploration is required. Encouragingly, the integration of Sb_2S_3 and Sb_2Se_3 into devices has yielded exciting results.[19,65,66] However, here we report on the material itself and, given the preliminary optical properties required, we firmly believe that this will motivate further optimization of the thin film as well as numerical and experimental studies employing GeSe as an ultra-low loss PCM in various reconfigurable devices, which is well beyond the scope of the present study.

To complete the library of optical properties of these materials, we finally focused on $GeSe_{1-x}Te_x$ nonlinear optical properties. Hence, we computed the Kerr refractive indices n_2 for all thin films in the amorphous phase using the Sheik-Bahae model.[38] The occurrence of nonlinearity in the refractive index for a dielectric material is associated with higher-order terms of susceptibility (χ) that become non-negligible for a sample under the influence of an intense applied electromagnetic field. The refractive index can therefore be expressed as $n = n_0 + n_2 <E^2>$, where n_0 and n_2 are the linear and the nonlinear Kerr refractive indices, respectively, and $<E^2>$ is the mean square value of the electric field of the optical incident beam. The Sheik–Bahae model is an analytical approach that estimates the nonlinear index, n_2, from the linear refractive index value, n, and the optical bandgap energy E_g^{04}, identified as the energy where the absorption coefficient $\alpha = 4\pi\kappa/\lambda$ exceeds 10^4 cm^{-1}.[67] Sellmeier equation is used to extrapolate the indices determined by VASE in the spectral range of transparency.[68] This approach enables us to estimate the n values up to 4 μm in the MIR since sudden changes in the refractive index behavior in that range are not expected. As we show in reference,[34] the Sheik–Bahae model can be accurate enough to get excellent qualitative trends on n_2 for chalcogenide materials. Therefore, calculated n_2 values for each $GeSe_{1-x}Te_x$ film with varying Te concentrations are plotted in **Figure 4**. For each $GeSe_{1-x}Te_x$ thin film composition, the data were
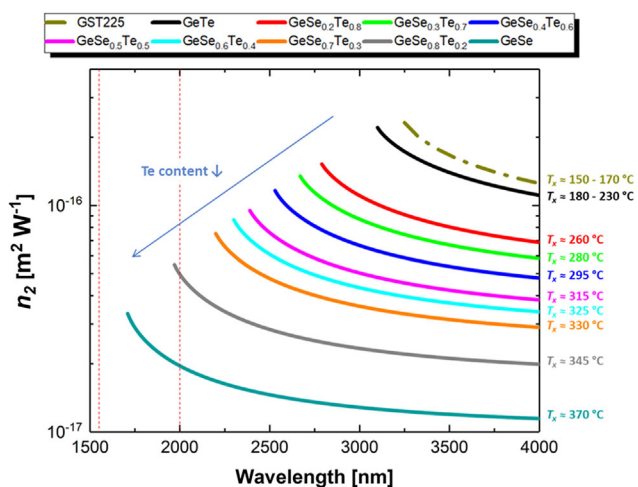
Figure 4. Nonlinear Kerr (n_2) refractive index as a function of wavelength for the amorphous as-deposited $GeSe_{1-x}Te_x$ thin films. The n_2 curves were obtained by means of Sheik–Bahae model (see text and references[33,34,38]). In each case, the data were plotted only in the spectral range for which the TPA losses are limited (see text).

plotted only in the wavelength/energy range for which the two-photon absorption (TPA) losses tend to zero which is mandatory for nonlinear photonic applications, hence for energies smaller than $E_g^{04}/2$. Very high n_2 values are obtained for all $GeSe_{1-x}Te_x$ amorphous films in the near-infrared (NIR)–MIR range, with maximum values and negligible TPA losses ranging from 3.3×10^{-17} m^2 W^{-1} for GeSe at 1710 nm to 2.2×10^{-16} m^2 W^{-1} at 3100 nm for GeTe. These values are at least two orders of magnitude higher than the silicon nitride (SiN) value estimated to be 2.0×10^{-19} m^2 W^{-1} and considered nowadays as the reference material for on-chip nonlinear NIR photonics applications.[33,34,69] Moreover, the Kerr index values increase with the increase of the Te atomic content from GeSe to GeTe and then to GST225. Similarly, the spectral range of interest (for which TPA losses are limited) shifts toward the MIR range when going from GeSe to GeTe and GST225. It must be emphasized that this trend was expected since the linear refractive indices in the transparent region increase and the energy gaps decrease when going from GeSe to GeTe and toward GST225. Therefore, it is worth noting that amorphous GST225 could also be considered as a promising candidate for nonlinear photonic applications at wavelengths higher than 3250 nm, where it presents a nonlinear refractive index of $n_2 = 2.3 \times 10^{-16}$ m^2 W^{-1}. However, this must be mitigated by its low thermal stability when compared to $GeSe_{1-x}Te_x$ compounds. As shown in Figure 4, GST225 exhibits a crystallization temperature (T_x) that can be as low as 150–170 °C (depending on whether or not the surface of the film is oxidized),[2] whereas that of $GeSe_{1-x}Te_x$ are much higher starting from $T_x \approx 180$–230 °C for GeTe (depending on whether or not the surface of the film is oxidized)[2] and going up to $T_x = 325$ °C for $GeSe_{0.49}Te_{0.51}$ and higher than 350 °C for $GeSe_{0.86}Te_{0.14}$.[40] Since nonlinear optical processes require high laser powers, which inevitably cause materials to heat up due to the absorption of residual contaminants, defects, and impurities, the thermal stability is essential for nonlinear photonics applications. To evaluate the experimental optical propagation losses and the optical-induced damages of our $GeSe_{1-x}Te_x$ alloys, we are working on device fabrication. This is challenging because of the challenging waveguides' fabrication process of etching for the $GeSe_{1-x}Te_x$ thin films. Besides, the etching requires optimized recipes for each alloy composition to produce suitable waveguides and grating couplers.

3. Conclusion

In conclusion, we have reported on the optical properties of $GeSe_{1-x}Te_x$ thin films as new PCMs that are very promising for on-chip low-/ultra-low-loss reconfigurable photonic applications and nonlinear devices. All $GeSe_{1-x}Te_x$ alloys described here, except covalently bonded GeSe, show a large refractive index contrast between amorphous and crystalline phases ($\Delta n > 1.7$) with a moderate change of extinction coefficients. For applications at telecommunication wavelengths based on phase change, these alloys have a FOM that exceeds up to 550% that of GST225 which is, for now, the standard PCM for nonvolatile reconfigurable photonics and that is up to three times higher than that of GSST2241.[17,23] We also show that controlling the Se/Te content in the alloys is a practical way to tune the material properties to suit

desired applications. The GeSe alloy shows a non-negligible index contrast between the amorphous and crystalline phases with a value of $\Delta n = 0.2$, accompanied by an ultra-low level of loss since the extinction coefficients for both phases are below our instrumental limit of sensitivity. This needs to be nuanced by the fact that GeSe thin film after crystallization presents some voids. As such, GeSe could be a good candidate for active phase modulation on a photonic chip, but further study and devices are needed to prove it. For nonlinear photonics applications, nonlinear Kerr refractive index n_2 values are reported for all $GeSe_{1-x}Te_x$ amorphous films in the NIR–MIR range. Maximum values with negligible TPA losses range from $3.3 \times 10^{-17}\,m^2\,W^{-1}$ for GeSe at 1710 nm to $2.2 \times 10^{-16}\,m^2\,W^{-1}$ at 3100 nm for GeTe. All largely exceed the n_2 values of standard nonlinear materials in integrated photonics. They also present a relatively good thermal stability which makes them attractive candidates for further developments in the field of nonlinear photonics such as for supercontinuum or frequency comb generation in the MIR. To evaluate the experimental optical propagation losses and the optical-induced damages of our $GeSe_{1-x}Te_x$ alloys, work on device fabrication is ongoing and will benefit from already available mature integration processes from phase-change memory, and ovonic threshold switching (OTS) selector devices fabrication.

4. Experimental Section

Thin Film Deposition: $GeSe_{1-x}Te_x$ thin films were deposited at room temperature by magnetron co-sputtering of pure GeSe and GeTe targets in an industrial cluster tool on silicon substrate (300 mm diameter) under Ar atmosphere. The power, pressure, and time of deposition were adjusted to deposit amorphous films with x varying from 0 to 1.

The deposited thin films were protected from surface oxidation by in situ deposition of 10 nm GeN_x capping layer obtained by reactive sputtering of a pure Ge target under $Ar + N_2$ atmosphere. The compositions of the amorphous as-deposited GeTe, GeSe, and $GeSe_{1-x}Te_x$ films were determined by wavelength-dispersive X-ray fluorescence (WDXRF). For GeTe film, the composition was found to be close to the nominal one with a slight excess of Ge as usual for this material deposited by sputtering.[2,70] For GeSe film, the composition is close to 50/50 within the error bars of about 1–2 at%. All the measured thin film compositions are summarized in **Table 1**.

Table 1. Ge, Se, and Te atomic concentrations (at%) determined by WDXRF for the thin films.

Sample label[a]	Ge [at%]	Se [at%]	Te [at%]
GeTe	53	–	47
$GeSe_{0.2}Te_{0.8}$	52.5	10	37.5
$GeSe_{0.3}Te_{0.7}$	52	15	33
$GeSe_{0.4}Te_{0.6}$	52	20	28
$GeSe_{0.5}Te_{0.5}$	51.3	25.3	23.4
$GeSe_{0.6}Te_{0.4}$	51	30	19
$GeSe_{0.7}Te_{0.3}$	50	35	15
GeSe	49	51	–

[a]The relative atomic composition is determined with a precision of ± 0.1 at%. The absolute error is ± 1–2 at% and it results from the calibration uncertainty in WDXRF measurements.

VASE measurements on the deposited films were carried out using a J. A. Woolam RC2 operating in the 210–2500 nm (i.e., 5.9–0.5 eV) range. Data were collected at three incidence angles equal to 60°, 65°, and 70° at room temperature on both amorphous thin films and the same samples after annealing up to 400 °C for $GeSe_{1-x}Te_x$ and up to 250 °C for GST225 (to obtain the FCC phase). Film thicknesses measured by X-ray reflectivity (XRR) were confirmed by VASE measurements that also allowed to extract the linear refractive index n, the extinction coefficient k and the optical bandgap E_g^{04} of each thin film sample. The thickness of the analyzed samples is of about 50 nm.

Spectroscopic ellipsometry is an indirect technique, and modeling of raw data is required to extract the optical parameters of the thin film samples. Experimental VASE raw data were fitted varying model parameters using CompleteEASE software. The imaginary part of the dielectric function $\varepsilon_2(E) = 2\,n(E).k(E)$ is calculated as the product of the variable band edge function and Lorentz oscillator function to obtain correct near-gap and above-gap optical responses. As variable edge function, Tauc–Lorentz[71,72] and Cody–Lorentz (CL)[73,74] were shown to be suitable for the description of the optical responses in amorphous semiconductors. However, CL model was selected in this study since it was already shown to be more appropriate for the description of the amorphous chalcogenide thin films' optical functions. In fact, it includes the correct band edge function and it possesses a gentle onset of absorption edge as it contains the localized states above the valence band given by the weak Urbach absorption tail.[75–77] To estimate the linear refractive indices of the samples from the measured ellipsometric angles (Ψ,Δ), we employed a four layers model consisting of: 1) surface roughness; 2) isotropic GeN_x capping layer (≈ 10 nm); 3) isotropic main layer of $GeSe_{1-x}Te_x$ or GST225; and 4) Si substrate. It is important to note that in all the cases, the thicknesses of the thin $GeSe_{1-x}Te_x$/GST225 films, and thicknesses of the surface roughness (assuming to be composed of thin film GeN_x and voids) and the GeN_x capping layer were fitted parameters as well. Drude-type contribution for free carriers was added to the CL model for the $GeSe_{1-x}Te_x$ crystallized films with $x \neq 0$, improving considerably the fitting accuracy. Regression analysis was performed by the root mean square error values minimization procedure.

Supporting Information

Supporting Information is available from the Wiley Online Library or from the author.

Conflict of Interest

The authors declare no conflict of interest.

Data Availability Statement

The data that support the findings of this study are available from the corresponding author upon reasonable request.

Keywords

[1] P. Noé, C. Vallée, F. Hippert, F. Fillot, J.-Y. Raty, *Semicond. Sci. Technol.* **2018**, *33*, 013002.

[2] A. Redaelli, in *Phase Change Memory*, Springer International Publishing, Cham **2018**.

[3] C. Ríos, M. Stegmaier, P. Hosseini, D. Wang, T. Scherer, C. D. Wright, H. Bhaskaran, W. H. P. Pernice, *Nat. Photonics* **2015**, *9*, 725.

[4] J. Feldmann, N. Youngblood, M. Karpov, H. Gehring, X. Li, M. Stappers, M. Le Gallo, X. Fu, A. Lukashchuk, A. S. Raja, J. Liu, C. D. Wright, A. Sebastian, T. J. Kippenberg, W. H. P. Pernice, H. Bhaskaran, *Nature* **2021**, *589*, 52.

[5] B. J. Eggleton, B. Luther-Davies, K. Richardson, *Nat. Photonics* **2011**, *5*, 141.

[6] S. Ghazi Sarwat, F. Brückerhoff-Plückelmann, S. G.-C. Carrillo, E. Gemo, J. Feldmann, H. Bhaskaran, C. D. Wright, W. H. P. Pernice, A. Sebastian, *Sci. Adv.* **2022**, *8*, eabn3243.

[7] P. Hosseini, C. D. Wright, H. Bhaskaran, *Nature* **2014**, *511*, 206.

[8] N. Farmakidis, N. Youngblood, X. Li, J. Tan, J. L. Swett, Z. Cheng, C. D. Wright, W. H. P. Pernice, H. Bhaskaran, *Sci. Adv.* **2019**, *5*, eaaw2687.

[9] A. Heßler, S. Wahl, T. Leuteritz, A. Antonopoulos, C. Stergianou, C.-F. Schön, L. Naumann, N. Eicker, M. Lewin, T. W. W. Maß, M. Wuttig, S. Linden, T. Taubner, *Nat. Commun.* **2021**, *12*, 924.

[10] A. Heßler, I. Bente, M. Wuttig, T. Taubner, *Adv. Opt. Mater.* **2021**, *9*, 2101118.

[11] B. Gholipour, J. Zhang, K. F. MacDonald, D. W. Hewak, N. I. Zheludev, *Adv. Mater.* **2013**, *25*, 3050.

[12] Y. Wang, P. Landreman, D. Schoen, K. Okabe, A. Marshall, U. Celano, H.-S. P. Wong, J. Park, M. L. Brongersma, *Nat. Nanotechnol.* **2021**, *16*, 667.

[13] L. Conrads, N. Honné, A. Ulm, A. Heßler, R. Schmitt, M. Wuttig, T. Taubner, *Adv. Opt. Mater.* **2023**, *11*, 2202696.

[14] L. Conrads, A. Heßler, K. G. Wirth, S. Meyer, M. Wuttig, D. N. Chigrin, T. Taubner, *Adv. Opt. Mater.* **2023**, *11*, 2300499.

[15] S. Abdollahramezani, O. Hemmatyar, M. Taghinejad, H. Taghinejad, A. Krasnok, A. A. Eftekhar, C. Teichrib, S. Deshmukh, M. A. El-Sayed, E. Pop, M. Wuttig, A. Alù, W. Cai, A. Adibi, *Nat. Commun.* **2022**, *13*, 1696.

[16] M. Y. Shalaginov, S. An, Y. Zhang, F. Yang, P. Su, V. Liberman, J. B. Chou, C. M. Roberts, M. Kang, C. Rios, Q. Du, C. Fowler, A. Agarwal, K. A. Richardson, C. Rivero-Baleine, H. Zhang, J. Hu, T. Gu, *Nat. Commun.* **2021**, *12*, 1225.

[17] M. Wuttig, H. Bhaskaran, T. Taubner, *Nat. Photonics* **2017**, *11*, 465.

[18] B. Gholipour, S. R. Elliott, M. J. Müller, M. Wuttig, D. W. Hewak, B. E. Hayden, Y. Li, S. S. Jo, R. Jaramillo, R. E. Simpson, J. Tominaga, Y. Cui, A. Mandal, B. J. Eggleton, M. Rochette, M. Rezaei, I. Alamgir, H. M. Shamim, R. Kormokar, A. Anjum, G. T. Zeweldi, T. S. Karnik, J. Hu, S. O. Kasap, G. Belev, A. Reznik, *J. Phys. Photonics* **2023**, *5*, 012501.

[19] C. Ríos, Q. Du, Y. Zhang, C.-C. Popescu, M. Y. Shalaginov, P. Miller, C. Roberts, M. Kang, K. A. Richardson, T. Gu, S. A. Vitale, J. Hu, *PhotoniX* **2022**, *3*, 26.

[20] N. Yamada, E. Ohno, K. Nishiuchi, N. Akahira, M. Takao, *J. Appl. Phys.* **1991**, *69*, 2849.

[21] M. Wuttig, N. Yamada, *Nat. Mater.* **2007**, *6*, 824.

[22] R. A. Soref, D. L. McDaniel, B. R. Bennett, *J. Light. Technol.* **1988**, *6*, 437.

[23] Q. Zhang, Y. Zhang, J. Li, R. Soref, T. Gu, J. Hu, *Opt. Lett.* **2018**, *43*, 94.

[24] Y. Zhang, J. B. Chou, J. Li, H. Li, Q. Du, A. Yadav, S. Zhou, M. Y. Shalaginov, Z. Fang, H. Zhong, C. Roberts, P. Robinson, B. Bohlin, C. Ríos, H. Lin, M. Kang, T. Gu, J. Warner, V. Liberman, K. Richardson, J. Hu, *Nat. Commun.* **2019**, *10*, 4279.

[25] S. Abdollahramezani, O. Hemmatyar, H. Taghinejad, A. Krasnok, Y. Kiarashinejad, M. Zandehshahvar, A. Alù, A. Adibi, *Nanophotonics* **2020**, *9*, 1189.

[26] R. Frerichs, *J. Opt. Soc. Am.* **1953**, *43*, 1153.

[27] A. R. Hilton, K. Sid, in *Chalcogenide Glasses for Infrared Optics*, The McGraw-Hill Companies, Inc., New York **2010**.

[28] F. Smektala, C. Quemard, L. Leneindre, J. Lucas, A. Barthélémy, C. De Angelis, *J. Non-Cryst. Solids* **1998**, *239*, 139.

[29] F. Smektala, C. Quemard, V. Couderc, A. Barthélémy, *J. Non-Cryst. Solids* **2000**, *274*, 232.

[30] J.-L. Adam, L. Calvez, J. Trolès, V. Nazabal, *Int. J. Appl. Glass Sci.* **2015**, *6*, 287.

[31] C. Gonçalves, R. Mereau, V. Nazabal, C. Boussard-Pledel, C. Roiland, E. Furet, M. Deschamps, B. Bureau, M. Dussauze, *J. Solid State Chem.* **2021**, *297*, 122062.

[32] A. Lemière, F. Désévédavy, P. Mathey, P. Froidevaux, G. Gadret, J.-C. Jules, C. Aquilina, B. Kibler, P. Béjot, F. Billard, O. Faucher, F. Smektala, *J. Opt. Soc. Am. B* **2019**, *36*, A183.

[33] J.-B. Dory, C. Castro-Chavarria, A. Verdy, J.-B. Jager, M. Bernard, C. Sabbione, M. Tessaire, J.-M. Fédéli, A. Coillet, B. Cluzel, P. Noé, *Sci. Rep.* **2020**, *10*, 11894.

[34] J.-B. Dory, M. Ibnoussina, J.-Y. Raty, J.-B. Jager, A. Verdy, A. Coillet, P. Colman, A. Albanese, M. Tomelleri, B. Cluzel, P. Noé, *Adv. Opt. Mater.* **2023**, *11*, 2301154.

[35] M. Baillieul, E. Baudet, K. Michel, J. Moreau, P. Němec, K. Boukerma, F. Colas, J. Charrier, B. Bureau, E. Rinnert, V. Nazabal, *Sensors* **2021**, *21*, 2449.

[36] P. T. Lin, H.-Y. G. Lin, Z. Han, T. Jin, R. Millender, L. C. Kimerling, A. Agarwal, *Adv. Opt. Mater.* **2016**, *4*, 1755.

[37] S. Dai, F. Chen, Y. Xu, Z. Xu, X. Shen, T. Xu, R. Wang, W. Ji, *Opt. Express* **2015**, *23*, 1300.

[38] M. Sheik-Bahae, D. C. Hutchings, D. J. Hagan, E. W. Van Stryland, *IEEE J. Quantum Electron.* **1991**, *27*, 1296.

[39] M. Ibnoussina, A. Coillet, J.-B. Dory, J.-B. Jager, P. Colman, B. Cluzel, *Opt. Lett.* **2020**, *45*, 5053.

[40] M. Tomelleri, F. Hippert, T. Farjot, C. Licitra, N. Vaxelaire, J.-B. Dory, D. Benoit, V. Giordano, P. Noé, *Phys. Status Solidi RRL* **2021**, *15*, 2000451.

[41] B. J. Kooi, M. Wuttig, *Adv. Mater.* **2020**, *32*, 1908302.

[42] M. Zhu, O. Cojocaru-Mirédin, A. M. Mio, J. Keutgen, M. Küpers, Y. Yu, J.-Y. Cho, R. Dronskowski, M. Wuttig, *Adv. Mater.* **2018**, *30*, 1706735.

[43] L. Guarneri, S. Jakobs, A. Hoegen, S. Maier, M. Xu, M. Zhu, S. Wahl, C. Teichrib, Y. Zhou, O. Cojocaru-Mirédin, M. Raghuwanshi, C. Schön, M. Drögeler, C. Stampfer, R. P. S. M. Lobo, A. Piarristeguy, A. Pradel, J. Raty, M. Wuttig, *Adv. Mater.* **2021**, *33*, 2102356.

[44] J. Raty, M. Schumacher, P. Golub, V. L. Deringer, C. Gatti, M. Wuttig, *Adv. Mater.* **2019**, *31*, 1806280.

[45] M. Wuttig, V. L. Deringer, X. Gonze, C. Bichara, J.-Y. Raty, *Adv. Mater.* **2018**, *30*, 1803777.

[46] K. Ren, M. Zhu, W. Song, S. Lv, M. Xia, Y. Wang, Y. Lu, Z. Ji, Z. Song, *Nanoscale* **2019**, *11*, 1595.

[47] D. Xia, Z. Yang, P. Zeng, B. Zhang, J. Wu, Z. Wang, J. Zhao, J. Huang, L. Luo, D. Liu, S. Yang, H. Guo, Z. Li, *Laser Photonics Rev.* **2023**, *17*, 2200219.

[48] J. Pan, D. Xia, Z. Wang, B. Zhang, Z. Li, *J. Light. Technol.* **2023**, *41*, 4065.

[49] H. Dieker, M. Wuttig, *Thin Solid Films* **2005**, *478*, 248.

[50] H. J. Kim, J. Sohn, N. Hong, C. Williams, W. Humphreys, *J. Phys. Photonics* **2021**, *3*, 024008.

[51] K. Shportko, S. Kremers, M. Woda, D. Lencer, J. Robertson, M. Wuttig, *Nat. Mater.* **2008**, *7*, 653.

[52] C. Koch, G. Schienke, M. Paulsen, D. Meyer, M. Wimmer, H. Volker, M. Wuttig, W. Bensch, *Chem. Mater.* **2017**, *29*, 9320.

[53] A. C. Galca, F. Sava, I. D. Simandan, C. Bucur, V. Dumitru, C. Porosnicu, C. Mihai, A. Velea, *J. Non-Cryst. Solids* **2018**, *499*, 1.

[54] S. K. Bahl, K. L. Chopra, *J. Appl. Phys.* **1969**, *40*, 4940.

[55] S. K. Behal, G. N. Srivastava, *Thin Solid Flims* **1978**, *48*, 51.

[56] Z. Černošek, E. Černošková, M. Hejdová, J. Holubová, R. Todorov, *J. Non-Cryst. Solids* **2017**, *460*, 169.

[57] L. Yang, G. J. Zhou, *Chalcogenide Lett.* **2023**, *20*, 1.

[58] K. A. Aly, *J. Non-Cryst. Solids* **2009**, *355*, 1489.

[59] C. Williams, N. Hong, M. Julian, S. Borg, H. J. Kim, *Opt. Express* **2020**, *28*, 10583.

[60] M. N. Julian, C. Williams, S. Borg, S. Bartram, H. J. Kim, *Optica* **2020**, *7*, 746.

[61] K. Aryana, H. J. Kim, M. R. Islam, N. Hong, C.-C. Popescu, S. Makarem, T. Gu, J. Hu, P. E. Hopkins, *Opt. Mater. Express* **2023**, *13*, 3277.

[62] R. Soref, *Nat. Photonics* **2015**, *9*, 358.

[63] M. Delaney, I. Zeimpekis, D. Lawson, D. W. Hewak, O. L. Muskens, *Adv. Funct. Mater.* **2020**, *30*, 2002447.

[64] Z. Fang, J. Zheng, A. Saxena, J. Whitehead, Y. Chen, A. Majumdar, *Adv. Opt. Mater.* **2021**, *9*, 2002049.

[65] R. Chen, Z. Fang, C. Perez, F. Miller, K. Kumari, A. Saxena, J. Zheng, S. J. Geiger, K. E. Goodson, A. Majumdar, *Nat. Commun.* **2023**, *14*, 3465.

[66] M. Delaney, I. Zeimpekis, H. Du, X. Yan, M. Banakar, D. J. Thomson, D. W. Hewak, O. L. Muskens, *Sci. Adv.* **2021**, *7*, eabg3500.

[67] A. Zakery, S. R. Elliott, in *Optical Nonlinearities in Chalcogenide Glasses and their Applications*, Springer, Berlin **2007**.

[68] H. G. Dantanarayana, N. Abdel-Moneim, Z. Tang, L. Sojka, S. Sujecki, D. Furniss, A. B. Seddon, I. Kubat, O. Bang, T. M. Benson, *Opt. Mater. Express* **2014**, *4*, 1444.

[69] A. L. Gaeta, M. Lipson, T. J. Kippenberg, *Nat. Photonics* **2019**, *13*, 158.

[70] P. Noé, C. Sabbione, N. Bernier, N. Castellani, F. Fillot, F. Hippert, *Acta Mater.* **2016**, *110*, 142.

[71] G. E. Jellison, F. A. Modine, *Appl. Phys. Lett.* **1996**, *69*, 371.

[72] G. E. Jellison, F. A. Modine, *Appl. Phys. Lett.* **1996**, *69*, 2137.

[73] G. D. Cody, in *Hydrogenated Amorphous Silicon* (Ed: J. I. Pankove), Elsevier, Orlando **1984**, pp. 11–82.

[74] A. S. Ferlauto, G. M. Ferreira, J. M. Pearce, C. R. Wronski, R. W. Collins, X. Deng, G. Ganguly, *J. Appl. Phys.* **2002**, *92*, 2424.

[75] J. Orava, T. Wágner, J. Šik, J. Přikryl, M. Frumar, L. Beneš, *J. Appl. Phys.* **2008**, *104*, 043523.

[76] P. Němec, A. Moreac, V. Nazabal, M. Pavlišta, J. Přikryl, M. Frumar, *J. Appl. Phys.* **2009**, *106*, 103509.

[77] P. Němec, J. Přikryl, V. Nazabal, M. Frumar, *J. Appl. Phys.* **2011**, *109*, 073520.